ELSEVIER

Journal of Alloys and Compounds 279 (1998) 295–300

Journal of ALLOYS AND COMPOUNDS

Effect of microstructure, composition and non-stoichiometry on electrochemical properties of low-Co rare-earth nickel hydrogen storage alloys

Wei-Kang Hu*

Department of Structural Chemistry, Arrhenius Laboratory, Stockholm University, Stockholm S-106 91, Sweden

Received 29 May 1998

Abstract

A series of low-Co stoichiometric and non-stoichiometric rare-earth nickel hydrogen storage alloys were examined for the possible application as negative electrodes in NiMH batteries. Partial substitution of Co by one transitional metal such as Cu, Fe, Cr or Zn did not effectively improve the electrochemical cycling stability, while a combined replacement of Co by Cr, Cu and Si was very effective in improving the cycling durability though the initial capacity was slightly low as compared with the parent alloy. In this work, the low-Co non-stoichiometric alloys did not appear superior in the capacity, rate capability and the charge–discharge cycling stability. The discharge capacity seems to be determined by the alloying components and compositional homogeneity. The cycling durability was dominated by the microstructure of alloys. The microstructure and chemical composition of alloys were examined and analyzed by scanning electron microscopy (SEM) and electron probe microanalysis (EPMA). The relationship between the microstructure and electrochemical properties of alloys was discussed.

Keywords: Low-Co rare-earth nickel hydride alloy; Alloy microstructure; Stoichiometry and non-stoichiometry; Electrochemical hydrogen storage property

1. Introduction

Mm-based alloys have been investigated extensively as the negative electrodes of NiMH rechargeable batteries [1–3]. A typical composition of the presently used Mm-based alloy in NiMH batteries is $MmNi_{3.55}Co_{0.75}Mn_{0.4}Al_{0.3}$. In the commercial composition, cobalt is one of the most important alloying elements and also the most expensive metal. It almost takes up about 40–50% of the total cost of the alloy materials. Therefore, it is very essential to develop low cost Mm-based alloys with low-Co or without Co in order to reduce the cost of NiMH batteries and enhance the competition of NiMH batteries on the rechargeable battery market. However, the electrochemically cycling stability for the low-Co or Co-free Mm-based alloys was usually unsatisfactory [4–6]. For this reason, cobalt was thought to be the most important component for obtaining satisfactorily cycling lives of Mm-based alloy electrodes. In order to improve the durability of low-Co alloys, we recently reported a two-phase, multi-component low-Co Mm-based alloy with reasonable capacity and good cycling stability [7].

In this work, some stoichiometric and non-stoichiometric low-Co Mm-based alloys were further examined for the possible application as negative electrodes in NiMH batteries. The electrochemical behaviors such as capacity, cycling stability and rate capability, and the effect of the alloy microstructure and stoichiometry on the hydrogen absorbing properties were investigated and discussed.

2. Experimental details

For comparison, the higher Co-containing $MmNi_{3.75}Co_{0.62}Mn_{0.36}Al_{0.27}$ alloy, having a composition close to the commercial composition of $MmNi_{3.55}Co_{0.75}Mn_{0.4}Al_{0.3}$, was investigated. The other alloy compositions examined in this work are presented in Table 1. The composition of mischmetal used in this study is 78% La, 7.40% Ce, 2.24% Nd, 10.68% Pr, 0.36% Fe and 0.1% Mn. All alloys were prepared by arc-melting on a water-cooled copper hearth under an argon atmosphere and remelted four times to ensure good homogeneity. The

*Corresponding author.

0925-8388/98/$ – see front matter
PII: S0925-8388(98)00689-6

Table 1
Lattice parameters and electrochemical properties of low-Co Mm-based alloys

Alloy No.	Chemical composition	Lattice constant		Cell volume ($Å^3$)	Capacity ($mAh\ g^{-1}$)	Capacity decay $(C_{max}-C_{300})/C_{max}$
		a(Å)	c(Å)			
162	$MmNi_{3.75}Co_{0.42}Mn_{0.36}Al_{0.27}Cu_{0.2}$	a=5.036	c=4.054	89.04	305	33.5[a]
161	$MmNi_{3.75}Co_{0.42}Mn_{0.36}Al_{0.27}Cr_{0.2}$	a=5.040	c=4.034	88.74	300	29.25[a]
164	$MmNi_{3.75}Co_{0.42}Mn_{0.36}Al_{0.27}Fe_{0.2}$	a=5.032	c=4.047	88.73	292	
165	$MmNi_{3.75}Co_{0.42}Mn_{0.36}Al_{0.27}Zn_{0.2}$	a=5.028	c=4.026	88.13	285	
174	$MmNi_{3.65}Co_{0.22}Mn_{0.36}Al_{0.27}Cu_{0.4}Si_{0.1}$	a=5.040	c=4.040	88.87	280	29.8[a]
182	$MmNi_{3.65}Co_{0.22}Mn_{0.36}Al_{0.27}Cu_{0.5}Si_{0.1}$	a=5.030	c=4.035	88.41	268	31.8
183	$MmNi_{3.65}Co_{0.22}Mn_{0.36}Al_{0.27}Cu_{0.6}Si_{0.1}$	a=5.030	c=4.034	88.39	224	
170	$MmNi_{3.65}Co_{0.22}Mn_{0.36}Al_{0.27}Cr_{0.2}Cu_{0.2}Si_{0.1}$	a=5.030	c=4.066	89.10	273	25.6
186	$MmNi_{3.75}Co_{0.62}Mn_{0.36}Al_{0.27}$	a=5.040	c=4.038	88.83	314	24.4

[a] Capacity decay after 250 cycles.

as-prepared alloy samples were mechanically pulverized and screened into a different size. The alloy powders with a size of less than 38 μm were used for the crystallographic examination by X-ray powder diffraction (XRD), and those with a size of 45–75 μm for electrochemical measurements. For the microstructure characterization, a bulk sample was embedded in epoxy resin and the surface was subsequently polished in various successive steps mirror-like appearance. The surface morphology was studied by scanning electron microscopy (SEM), and the chemical composition was determined using electron probe X-ray microanalysis (EPMA).

Electrode properties of the alloys were tested in a half-cell with 6 M KOH solution at 30°C. A $Ni(OH)_2$ electrode (sintered) with a larger capacity and a Hg/HgO (6 M KOH) electrode were used as the counter-electrode and reference electrode, respectively. The MH electrodes were prepared by mechanically pressing (200 kg cm^{-2}) the well mixed alloy powders (~70%) with fine Ni powder (~17%), carbon black (~5%) and binding polymer on a nickel foam (size: 1.8×1.8 cm) at room temperature. Electrodes were charged at 0.25C rate for 5 h and discharge at 0.2C rate to a cut-off potential of −0.74 V vs. Hg/HgO electrode for activation. The cycling stability examination was conducted by charging at 1.0C rate for 1.2 h and discharging at the same rate to end potential of −0.74 V vs. Hg/HgO electrode using a computer controlled battery cycler in 6 M KOH at 30°C.

The electrochemical impedance spectroscopy (EIS) was carried out using an EG and G Princeton Applied Research potentiostat /galvanostat Model 273A and a solartron SI 1255 frequency response analyzer. The EIS experiments were performed after more than ten charge–discharge cycles. The amplitude of the Sine perturbation signal was 5 mV. The frequency was scanned from the highest (1×10^4 Hz) to the lowest value (1×10^{-3} Hz).

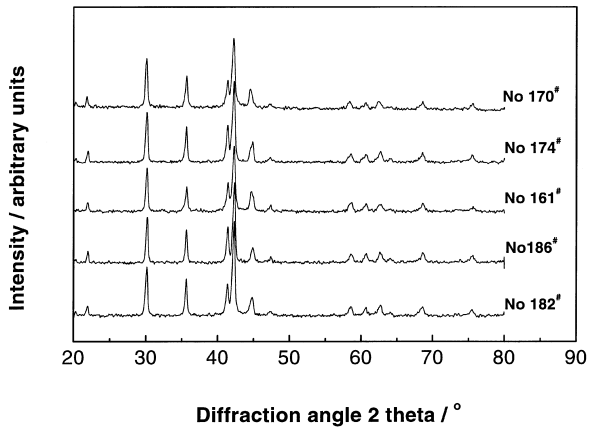

Fig. 1. X-ray powder diffraction patterns for five representative alloys.

3. Results and discussion

3.1. Crystal structure and microprobe analysis

Fig. 1 shows the X-ray powder diffraction patterns of the five representative alloys. The five alloys show almost the same patterns and seem to be single phase with the hexagonal $CaCu_5$ crystal structure. The lattice parameters and unit cell volumes for all alloys are summarized in Table 1. Fig. 2 shows the scanning electron microscopy images of the five alloys. It could be seen from Fig. 2 that only No 186# and No 174# alloys give an homogenous compositional distribution and are confirmed to be single phase. In contrast, the other three alloys do not give a uniform composition and exhibit two phases. Microprobe analysis showed that the secondary phase for the No 170# alloy, which corresponds to the black area in Fig. 2(c), was predominantly rich in Cr with small amounts of Mn, Co and Ni. The secondary phase formed a three-dimensional network and served the function of microencapsulating the main phase grain (light grey). For the No 182# alloy, a Mm-rich Ni-poor precipitated phase with $MmNi_{0.80}Co_{0.02}Mn_{0.15}Al_{0.1}Cu_{0.12}Si_{0.06}$ composition (white area) as shown in Fig. 2(e) was observed, which precipitated dispersively in the main phase. The main phase consisted of the $MmNi_{3.20}Co_{0.15}Mn_{0.53}Al_{0.27}Cu_{0.49}Si_{0.13}$ composition with hexagonal $CaCu_5$ structure. For the No 161# alloy, a

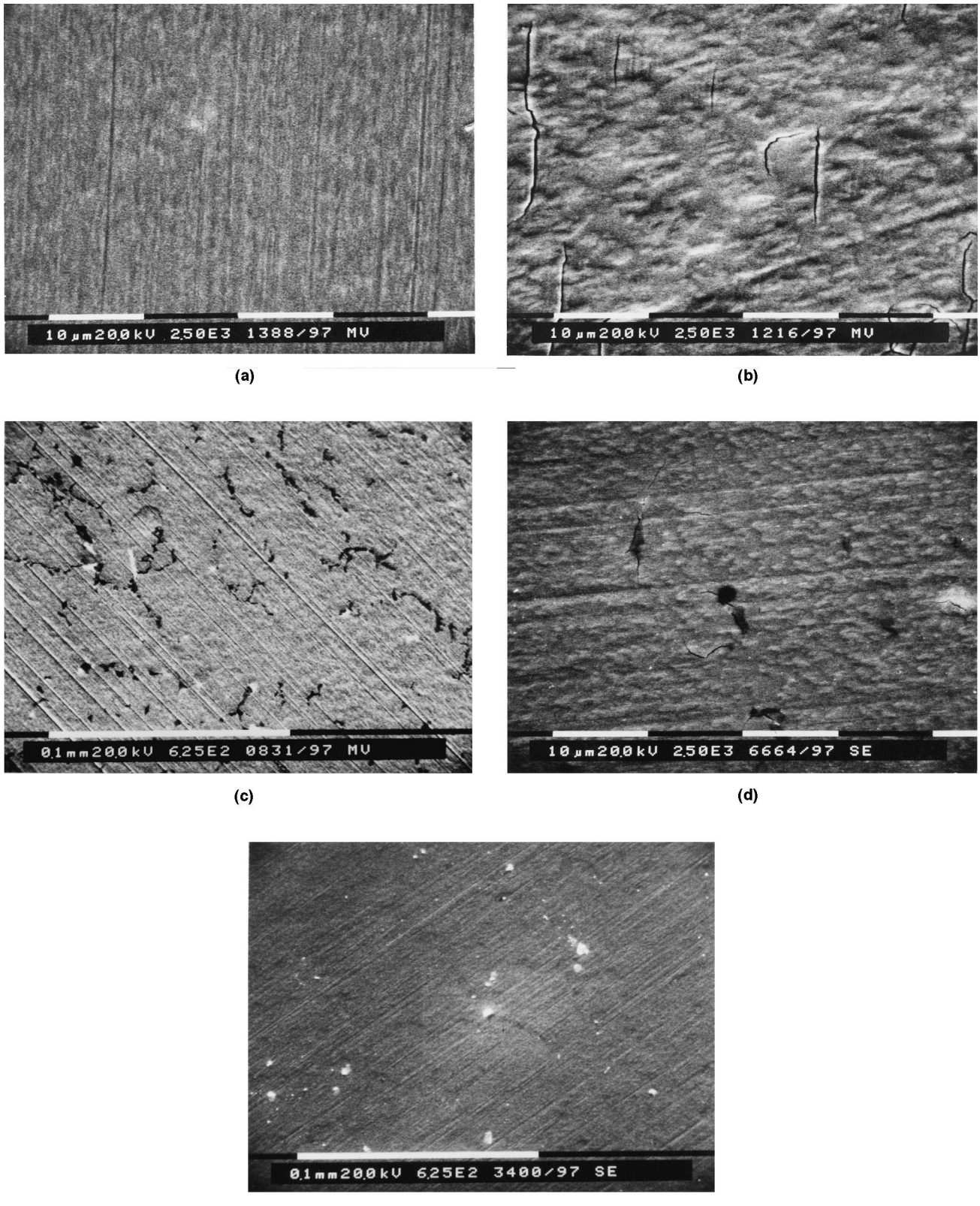

Fig. 2. SEM images for the five alloys. (a) $MmNi_{3.75}Co_{0.62}Mn_{0.36}Al_{0.27}$ alloy, (b) $MmNi_{3.65}Co_{0.22}Mn_{0.36}Al_{0.27}Cu_{0.4}Si_{0.1}$ alloy, (c) $MmNi_{3.65}Co_{0.22}Mn_{0.36}Al_{0.27}Cr_{0.2}Cu_{0.2}Si_{0.1}$ alloy, (d) $MmNi_{3.75}Co_{0.42}Mn_{0.36}Al_{0.27}Cr_{0.2}$ alloy, and (e) $MmNi_{3.65}Co_{0.22}Mn_{0.36}Al_{0.27}Cu_{0.5}Si_{0.1}$ alloy.

Cr-rich phase, which corresponds to the black area in Fig. 2(d), was present. The chemical compositions of the secondary phase or precipitated phase and the main phase for the three alloys are presented in Table 2. However, the secondary phases or precipitated phases for the three alloys could not be detected by XRD as shown in Fig. 1 due to their limited quantity. It is interesting to note that the Cr-containing alloys in this work facilitate the formation of a secondary phase. This trend was also observed in AB_2-type alloys by other investigators [8,9].

3.2. Electrochemical discharge feature

Fig. 3 shows the discharge curves of seven alloy electrodes after activation. The No 186# alloy has the highest capacity of about 314 mAh g^{-1}. The maximum capacity for the other alloys is summarized in Table 1. After partial replacement of Co by Cu, Cr, Fe or Zn, or partial replacement of Ni and Co by Cr, Cu and Si, the discharge capacity decreases compared with the parent alloy (No 186# alloy). The maximum capacity further decreases when the alloy composition changes from stoichiometry to non-stoichiometry as shown in Fig. 3(b). The influence of non-stoichiometric $A(B_5)_X$ alloys on the electrochemical properties has been investigated earlier [10–14]. Tadokoro [10] and Fukumoto [11] et al. found that Mm-rich $Mm(B_5)_X$ alloys within the composition range ($0.9 \leq X \leq 0.96$) showed higher discharge capacity than the stoichiometric alloys. Higashiyama et al. [14] studied the influence of Mm-poor $Mm(B_5)_X$ alloys on the discharge capacity and charge–discharge cycling stability, and found that the capacity was dominated by the stoichiometry. In our cases, the capacity seems to be determined by the alloying components and the compositional homogeneity. In Cr-containing alloys or non-stoichiometric alloys, the decrease in discharge capacity is partly ascribed to the formation of a secondary phase or precipitate. Fig. 4 shows the dependence of discharge capacity on cycle number for the secondary phase of the No 170# alloy. It can be clearly seen that the secondary phase was almost unable to absorb an amount of hydrogen. Therefore, the secondary phase or precipitated phase negatively influenced the discharge capacity of the alloys.

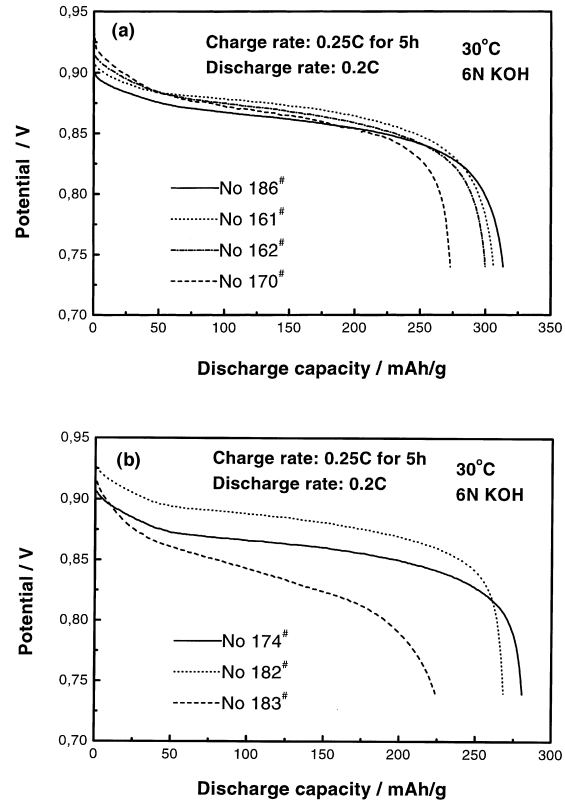

Fig. 3. (a) Discharge curves of five alloy electrodes in 6 M KOH at 30°C, (b) Discharge curves of three alloy electrodes in 6 M KOH at 30°C.

Table 2
Chemical compositions of the secondary phase and main phase for the three alloys

Alloy No.	Secondary phase Average composition (at %)	Main phase Average composition (at %)
170	Cr=82.13 Mn=3.41 Co=5.01 Ni=9.45	Al=60.4, Si=2.72 La=13.3, Ce=3.95 Cr=2.11, Mn=6.86 Co=2.24, Ni=60.49 Cu=2.28
182	Al=4.47, Si=2.73 La=34.06, Ce=10.23 Mn=6.62, Co=1.01 Ni=35.65, Cu=5.23	Al=4.62, Si=2.28 La=13.21, Ce=4.13 Mn=9.25, Co=2.64 Ni=55.40, Cu=8.46
161	La=3.35, Cr=75.40 Mn=2.60, Co=7.21 Ni=11.44	

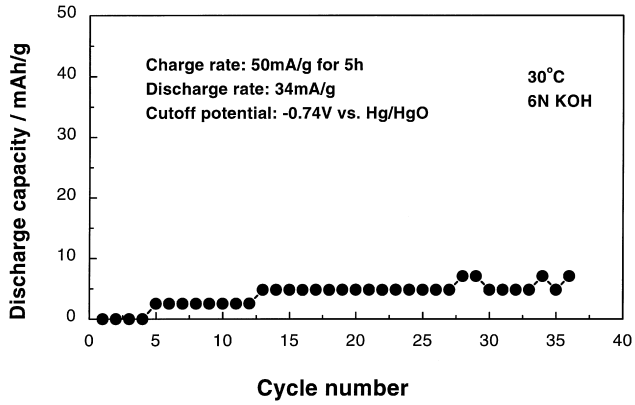

Fig. 4. The relationship between the discharge capacity and the cycle number for the alloy with the same chemical composition as the secondary phase of the No. 170# alloy.

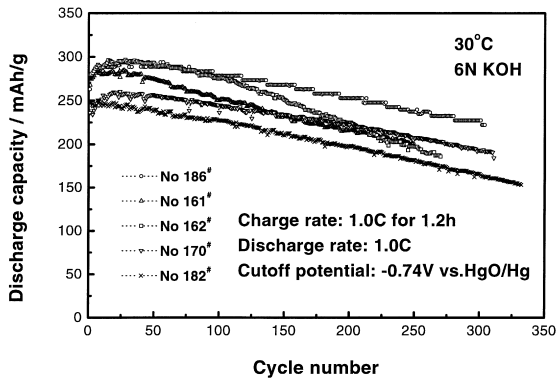

Fig. 5. The dependence of discharge capacity on the cycle number for the alloy electrodes. (a) $MmNi_{3.75}Co_{0.62}Mn_{0.36}Al_{0.27}$ alloy, (b) $MmNi_{3.75}Co_{0.42}Mn_{0.36}Al_{0.27}Cr_{0.2}$ alloy, (c) $MmNi_{3.75}Co_{0.42}Mn_{0.36}Al_{0.27}Cu_{0.2}$ alloy, (d) $MmNi_{3.65}Co_{0.22}Mn_{0.36}Al_{0.27}Cr_{0.2}Cu_{0.2}Si_{0.1}$ alloy, (e) $MmNi_{3.65}Co_{0.22}Mn_{0.36}Al_{0.27}Cu_{0.5}Si_{0.1}$ alloy.

3.3. Cycling stability and rate capability

Fig. 5 shows the relationship between the discharge capacity and the cycle number for five alloys. The capacity decay, the ratio of the maximum capacity to the capacity after 300 cycles, is chosen as a measure of the stability of alloys. The capacity decay for the examined alloys is presented in Table 1. The No 186# alloy showed the lowest value of the capacity decay. The No 170# alloy with low-Co content had almost same capacity decay as the No 186# alloy. It exhibited excellent cycling stability compared with the No 161#, 162#, 174# alloys. This indicated that the Cr, Cu and Si substitution in the No 170# alloy have a combined positive influence on the cycle life. It is well known that the cycling stability of alloys mainly depends on chemical compositions, alloy microstructure and preparatory methods of alloys. The No 170# alloy consists of two phases, as shown in Fig. 2(c), and the secondary phase (black area) is distributed between the grain boundaries of the main phase (light grey), which serves the function of microencapsulating the main phase grain. Therefore, the secondary phase in the No 170# alloy plays an important role in suppressing the degeneration of the alloy during repeating charge–discharge processes. In addition, according to Willems and other investigators [15–17], Si substitution in AB_5-type alloys can improve the cycling stability since the Si can form a closed surface oxide layer which effectively protects the inner hydride from oxidation. According to Notten et al. [12,13], the Cu-containing non-stoichiometric $La(Ni–Cu)_X$ alloys provided a larger improvement in the electrochemical cycling stability. Neutron diffraction investigations [18] also revealed that about 50% of the Cu atoms in Cu substituted alloys occupied the 2c Ni-site (plane $Z=0$) and Cu behaves in a similar way as Co. A fractional substitution of Cu for Ni is possibly favorable for the durability of an alloy. Taking account of above factors, the good cycling stability of the No 170# alloy is mainly ascribed to the alloy microstructure and the chemical composition.

For the non-stoichiometric alloys investigated in this work, however, the charge–discharge cycling stability did not appear superior to the stoichiometric alloys as seen from Table 1. As to the poor cycling durability of the non-stoichiometric alloys in this work, it could be related with the existence of a precipitated phase with Mm-rich Ni-poor composition as shown in Fig. 2(e) and Table 2. It was reported that some precipitates such as MmNi, Mn, Al–Ni alloys in non-stoichiometric Mm-based alloys would reduce the cycle performance due to their smaller durability against oxidation [19].

The dependence of the discharge capacity on the discharge rate for the examined alloys is shown in Fig. 6. As seen from the Fig. 6, the No 186# alloy exhibits the best rate capability. After partial replacement of Co by transitional metals, even for the non- stoichiometric alloys, the rate capability appears to be poorer than for the No 186# alloy. It is well known that cobalt in AB_5 alloy has a positive effect on cycle lives of alloy electrodes. In addition, cobalt is also an effective element in improvement of charge and discharge efficiencies of alloy electrodes. This is ascribed to the fact that cobalt can give the oxidized alloy surface a good electronic conductivity by a dissolution–precipitation process because cobalt hydroxide has a good electronic conductivity [5,20]. Therefore, alloys of higher Co concentration facilitate the improvement of high-rate charging and discharging. On the other hand, according to our EIS results as shown in Fig. 7, the No 186# alloy shows the smallest charge-transfer resistance than the other two low-Co alloys examined in this work.

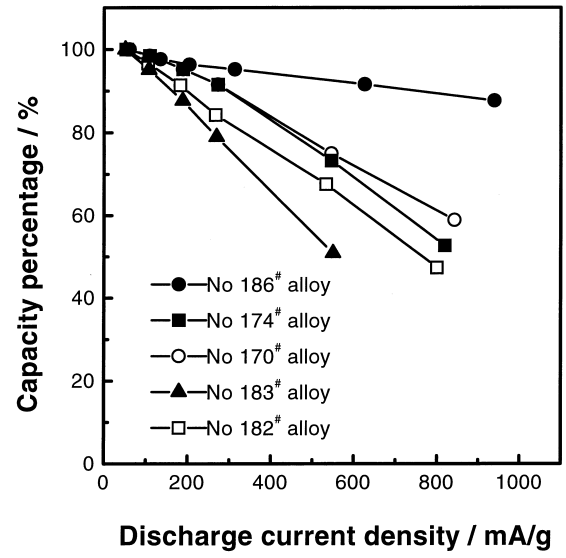

Fig. 6. The dependence of discharge capacity on the discharge current density for the alloy electrodes.

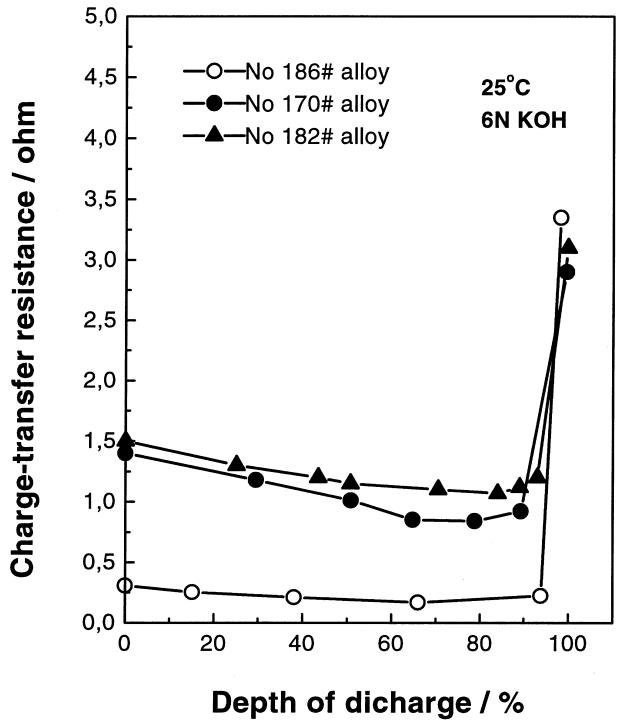

Fig. 7. The relationship between the charge-transfer resistance and the depth of discharge for three alloy electrodes.

This means that the No 186# alloy has the best hydride–dehydride kinetics and rate capability.

4. Conclusions

A series of low-Co multi-component Mm-based alloys aiming at reducing the raw material cost was prepared by arc-melting. The microstructure characteristics and electrochemical properties of these alloys were investigated. The conclusions are as follows:

The examination of the microstructure showed that the Cr-containing alloys facilitated the formation of a secondary phase.

Partial replacement of Co by one transitional metal such as Cu, Cr, Fe or Zn did not improve the electrochemically cycling stability. A combined replacement of Co by Cr, Cu and Si was very effective in improving the cycling durability. According to the results of microstructural analyses, the improvements of charge–discharge cycling stability for the No 170# alloy has mainly to be attributed to the secondary phase with the feature of a three-dimensional network.

A precipitate with Mm-rich Ni-poor composition was seen on the non-stoichiometric alloy surface, which was possibly responsible for the decrease of the cycling durability.

In this work, the alloys having over-stoichiometric compositions did not appear superior in capacity, cycling stability and rate capability.

According to our initial results above, it is possible to develop low-Co multi-component Mm-based alloys with satisfactory cycling stability and reasonable capacity for the low-cost NiMH batteries.

References

[1] H. Ogawa, M. Ikoma, H. Kawano, I. Matsumoto, Power Sources 12 (1989) 393.
[2] M. Ikoma, H. Kawano, I. Matsumoto, N. Yanagihara, Eur. Patent Appl. 0,271,043, 1987.
[3] T. Sakai, K. Muta, H. Miyamura, N. Kuriyama, H. Ishikawa, in: D.A. Corrigan, S. Srinivasan (Eds.), Proc. Symp. on Hydrogen Storage Materials, Batteries and Electrochemistry, Vol. 92–95, The Electrochem. Soc., NJ, 1992, p. 59.
[4] G.D. Adzic, J.R. Johnson, S. Mukerjee, J. McBreen, J.J. Reilly, J. Alloys Comp. 253–255 (1997) 579.
[5] T. Sakai, H. Miyamura, N. Kuriyama, H. Ishikawa, I. Uehara, Z. Phys. Chem. Bd183 (1994) 333.
[6] J.M. Cocciantelli, P. Bernard, S. Fernandez, J. Atkin, J. Alloys Comp. 253–254 (1997) 642.
[7] W.K. Hu, H. Lee, D.M. Kim, S.W. Jeon, J.Y. Lee, J. Alloys Comp. 268 (1998) 261.
[8] H. Miyamura, T. Sakai, N. Kuriyama, K. Oguro, I. Uehara, H. Ishikawa, Z. Phys. Chem. Bd83 (1994) 347.
[9] H. Miyamura, T. Sakai, N. Kuriyama, K. Oguro, A. Kato, H. Ishikawa, in: D.A. Corrigan, S. Srinivasan (Eds.), Proc. Symp. on Hydrogen Storage Materials Batteries and Electrochemistry, Vol. 92–95, The Electrochem. Soc., NJ, 1992, p. 179.
[10] M. Tadokoro, K. Moriwaki, K. Nishio, M. Nogami, N. Inoue, Y. Chikano, M. Kimoto, T. Ise, R. Maeda, F. Mizutaki, M. Takee, N. Furukawa, in: D.A. Corrigan, S. Srinivasan (Eds.), Proc. Symp. on Hydrogen Storage Materials Batteries and Electrochemistry, Vol. 92–95, The Electrochem. Soc., NJ, 1992, p. 92.
[11] Y. Fukumoto, M. Miyamoto, H. Inoue, M. Matsuoka, C. Iwakura, J. Alloys Comp. 231 (1995) 562.
[12] P.H.L. Notten, R.E.F. Einerhand, J.L.C. Daams, J. Alloys Comp. 210 (1994) 221.
[13] P.H.L. Notten, J.L.C. Daams, R.E.F. Einerhand, J. Alloys Comp. 210 (1994) 233.
[14] N. Higashiyama, Y. Matsura, H. Nogami, I. Yonezu, K. Nishio, J. Alloys Comp. 253–254 (1997) 648.
[15] J.J.G. Willems, K.H.J. Buschow, J. Less-Common Met. 129 (1987) 13.
[16] F. Meli, A. Züttel, L. Schlapbach, J. Alloys Comp. 190 (1992) 17.
[17] F. Meli, A. Züttel, L. Schlapbach, J. Alloys Comp. 202 (1993) 81.
[18] A. Percheron-Guegan, C. Lartigue, J.C. Achard, J. Less-Common Met. 109 (1985) 287.
[19] T. Sakai, H. Yoshinaga, H. Miyamura, N. Kuriyama, H. Ishikawa, J. Alloys Comp. 180 (1992) 37.
[20] M. Oshitani, H. Yufu, K. Takashima, S. Tsuji, Y. Matsumaru, J. Electrochem. Soc. 136 (1989) 1590.